Spectral averaged cross sections as a probe to a high energy tail of ^{235}U PFNS

Martin Schulc[1,*], Michal Kostal[1], Roberto Capote[2], Jan Simon[1], Tomas Czakoj[1], and Evzen Novak[1]

[1]Research Centre Rez Ltd, 250 68 Husinec-Rez 130, Czech Republic
[2]Nuclear Data Section, International Atomic Energy Agency, A-1400 Vienna, Austria

Abstract. The systematic evaluations of spectrum averaged cross sections of dosimetric reactions over a broad range of energies were performed in ^{252}Cf (spontaneous fission) and ^{235}U(n_{th},f) neutron fields. The neutron sources used in this study were LR-0, VR-1 zero power research light water reactors, LVR-15 10 MW research light water reactor, and ^{252}Cf neutron source with emission specified precisely by the manganese sulphate bath. All spectral averaged cross sections were inferred from measured reaction rates which were derived from gamma spectrometry. These gamma spectrometry measurements were performed using a single detector in all cases. The ratios of ^{252}Cf and ^{235}U spectral averaged cross sections can be used to specify the high energy tail of the ^{235}U prompt fission neutron spectrum that has ^{252}Cf spontaneous fission spectrum is considered as a standard. Furthermore, ratios are independent of cross section uncertainties since uncertainties in the cross sections are eliminated. Theoretical models of fission can be tested based on our measurements. The calculations were performed in MCNP6.2 transport code using different prompt fission neutron spectra and IRDFFII cross sections for threshold reactions. The ratios are in good agreement using only ENDF/B-VIII.0 ^{235}U prompt fission neutron spectrum suggesting it to be harder than in other evaluations.

1 Introduction

The ^{235}U prompt fission neutron spectrum (PFNS) is discrepant above 10 MeV since the existing differential experimental data above 10 MeV are contradictory [1]. State of the art ENDF/B-VIII.0 [2] and JEFF-3.3 [3] nuclear data libraries significantly differ in ^{235}U PFNS above 10 MeV, see Figure 1. On the contrary, ^{252}Cf(sf) is the only neutron standard. This source was used for the validation of dosimetric cross sections included in the IRDFF-II library [4]. Reliable estimation of ^{235}U PFNS is very important as it is used for the safety and regulatory applications in commercial fission reactors, reactor dosimetry, and also from the theoretical point of view.

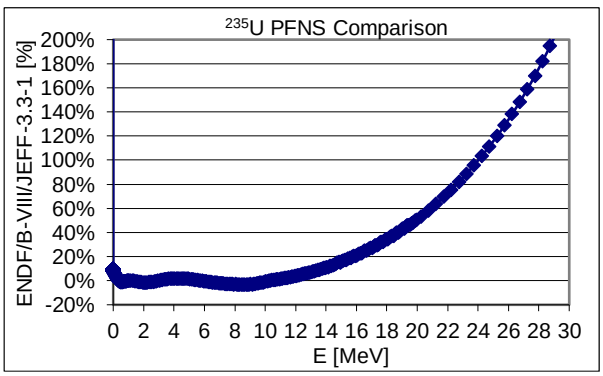

Fig. 1. Difference between ENDF/B-VIII.0 and JEFF-3.3 ^{235}U PFNS

The suitable quantity for assessing the high energy tail are spectral averaged cross sections (SACS) for dosimetric reactions since they are loaded with lower uncertainties than differential data. As the ^{252}Cf(sf) is the neutron standard, the SACS in its spectrum can be assumed as precisely determined. The ratios of ^{235}U and ^{252}Cf SACS can then help for a better estimation of the ^{235}U PFNS shape. Furthermore, ratios are independent of cross section uncertainties since uncertainties in the cross sections are eliminated.

The systematic evaluations of spectrum averaged cross sections of dosimetric reactions over a broad range of energies were performed in ^{252}Cf (spontaneous fission) and ^{235}U(nth,f) neutron fields. All spectral averaged cross sections were inferred from measured reaction rates which were derived from gamma spectrometry. These gamma spectrometry measurements were performed using a single detector in all cases.

2 Experimental and calculation methods

2.1 Neutron sources description

The neutron sources used for SACS estimations in experiments were: LR-0, VR-1 and LVR-15 light water reactors, and ^{252}Cf isotopic source.

* Corresponding author: martin.schulc@cvrez.cz

The LR-0 research reactor is a zero-power light water pool type reactor. The specially designed reference core [5] consists of six uranium fuel assemblies with nearly 3.3% ^{235}U enrichment surrounding a dry assembly with activation foils to be irradiated. Used fuel assemblies are the same as VVER-1000 type in the radial direction but in the axial direction, they are shortened to 125 cm. Reactor criticality is achieved by variation of a light water level only. Characterization of the special core was performed by the experiments dealing with reactivity characterization [6], fission rates distribution [7], and also neutron spectra measurements using a stilbene scintillation detector [8]. Details about SACS measurements in LR-0 can be found in [9], [10], [11].

The VR-1 research reactor is also a light water, zero-power pool-type reactor located in Prague. The core consists of tubular fuel assemblies of LRT-4M type enriched to 19.75 wt. % of ^{235}U, and contains several dry vertical channels with different diameters up to 90 mm and one radial channel with a diameter of 250 mm. The activation targets were placed in the center of a 25 mm channel located in the center of the fuel assembly positioned close to the radial channel of the reactor. The criticality of the reactor during irradiation was managed by the moving of the control rods. The details of the experiments and SACS measurements can be found in [12].

Unlike above mentioned zero power reactors, LVR-15 is a 10 MW reactor with forced cooling. As well as the VR-1 reactor, LVR-15 employs LRT-4M fuel with an enrichment of 19.7% of ^{235}U. The fuel has a burn-up due to the high operating power. Fuel composition is calculated using an onsite developed code NODER [13]. The measurement of SACS was performed near the fuel, where a high flux of high energy neutrons is achieved [14].

The ^{252}Cf isotopic source involved in ^{252}Cf experiments had initial emission of $(5.31 \pm 0.11) \cdot 10^8$ n/s. The emission was measured in the National Physical Laboratory, UK by means of a manganese sulphate bath. The experiments were performed during source emission between 2.9E8 n/s and 8.0E8 n/s. The experimental uncertainties and irradiation geometry of low and high volume sources were extensively described in [15]. The performed set of experiments involving ^{252}Cf was described in [16-19].

2.2 Calculation methods

All irradiated samples were measured using a single high purity germanium (HPGe) detector in a vertical configuration (ORTEC GEM35P4). The experimental reaction rates were derived from the Net Peak Areas (NPA) measured using the HPGe detector. These reaction rates were used to derive the SACS by means of the following equation:

$$q = \frac{C(T_m)\lambda T_m}{\eta \varepsilon N k T_l} \frac{1}{e^{-\lambda \Delta T}} \frac{1}{1-e^{-\lambda T_m}} \frac{1}{1-e^{-\lambda T_{irr}}}, \quad (1)$$

where: q is the experimental reaction rate per atom per second, N is the number of target isotope nuclei, ε is the detector efficiency, η is gamma branching ratio, λ is the decay constant, k characterizes the abundance of isotope of interest in the target and its purity, ΔT is the time between the end of irradiation and start of measurement, $C(T_m)$ is the measured number of counts, T_m is the real time of measurement by HPGe, T_l is the live time of measurement by HPGe (it is time of measurement corrected to the dead time of the detector), and T_{irr} is the time of irradiation. The coincidence summing was estimated for each sample separately. The method of efficiency calculation is described in [9].

The SACS is derived from reaction rate by correction factor C which considers the spectral shift effect, flux loss, and self-shielding together. The correction is computed by means of MCNP [20] as a ratio between the SACS in the real-setup and the SACS in the same setup consisting of void cells. The SACS are derived via Equation 2:

$$\overline{\sigma} = \frac{\int_{E\mathrm{thr}}^{E\max} \varphi(\mathrm{E})\sigma(\mathrm{E})dE}{\int_{E\mathrm{thr}}^{E\max} \varphi(\mathrm{E})dE} \times C, \quad (2)$$

where C denotes the correction factor, $\varphi(E)$ is the calculated neutron spectrum, $\sigma(E)$ is the cross section and $\overline{\sigma}$ denotes SACS.

3 Results

Table 1 shows differences between measured ^{235}U SACS and calculation using JEFF-3.3 ^{235}U PFNS. Disagreement with experiment was found for ^{89}Y(n,2n)^{88}Y, ^{19}F(n,2n)^{18}F, ^{58}Ni(n,2n)^{57}Ni, and ^{23}Na(n,2n)^{22}Na reactions. These reactions have high mean response energy (E50%). E50% is the energy where integration of the product of spectra and cross section reaches 50%. Table 2 shows differences between measured ^{235}U SACS and calculation using ENDF/B-VIII.0 ^{235}U PFNS. Agreement within uncertainties is achieved for all reactions. Figure 2 shows ^{252}Cf over ^{235}U SACS ratios in dependence on mean response energy. The plotted experimental data are listed in Table 3. The experimental results agree very well with calculated data using ^{235}U ENDF/B-VIII.0 PFNS unlike JEFF-3.3 which has a much softer neutron spectrum. The difference is clearly visible in E50% above 14 MeV. The difference between these two evaluations is approximately 20 % for reaction ^{23}Na(n,2n)^{22}Na (E50%=15.37 MeV).

Figure 3 displays comparison of ENDF/B-VIII.0 ^{235}U SACS with differential data by Staples [21]. The agreement is very good up to 12 MeV, then the agreement worsens with higher energies. The experimental data are up to 10 times higher for 16 MeV.

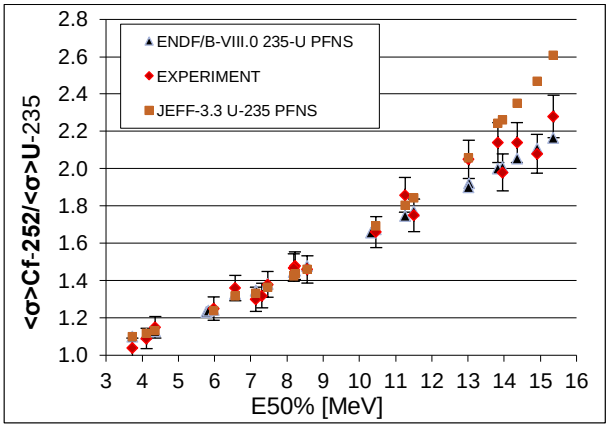

Fig. 2. Ratios of SACS in dependence on mean response energy

Table 1. Comparison of SACS using ^{235}U JEFF-3.3 PFNS.

Reaction	E50% [MeV]	Difference [%]	Unc. [%]
^{47}Ti(n,p)^{47}Sc	3.73	-0.16	3.9
^{58}Ni(n,p)^{58}Co	4.12	-0.36	3.5
^{46}Ti(n,p)^{46}Sc	5.98	0.14	4.0
^{56}Fe(n,p)^{56}Mn	7.46	1.21	3.2
^{48}Ti(n,p)^{48}Sc	8.22	1.07	4.2
^{197}Au(n,2n)^{196}Au	10.47	-1.23	4.7
^{127}I(n,2n)^{126}I	11.51	-3.85	5.5
^{89}Y(n,2n)^{88}Y	13.84	-10.77	4.6
^{19}F(n,2n)^{18}F	13.96	-11.26	3.8
^{58}Ni(n,2n)^{57}Ni	14.91	-14.69	4.5
^{23}Na(n,2n)^{22}Na	15.37	-17.07	5.4

Table 2. Comparison of SACS ^{235}U using ENDF/B-VIII.0 PFNS.

Reaction	E50% [MeV]	Difference [%]	Unc. [%]
^{47}Ti(n,p)^{47}Sc	3.73	3.48	3.9
^{58}Ni(n,p)^{58}Co	4.12	1.76	3.5
^{46}Ti(n,p)^{46}Sc	5.98	-0.74	4.0
^{56}Fe(n,p)^{56}Mn	7.46	0.76	3.2
^{48}Ti(n,p)^{48}Sc	8.22	0.74	4.2
^{197}Au(n,2n)^{196}Au	10.47	1.20	4.7
^{127}I(n,2n)^{126}I	11.51	1.04	5.5
^{89}Y(n,2n)^{88}Y	13.84	-0.52	4.6
^{19}F(n,2n)^{18}F	13.96	-2.71	3.8
^{58}Ni(n,2n)^{57}Ni	14.91	2.16	4.5
^{23}Na(n,2n)^{22}Na	15.37	2.36	5.4

Table 3. Reactions mean response energies with experimental SACS ratios and their uncertainties.

Reaction	E50% [MeV]	SACS Ratio	Unc. [%]
^{47}Ti(n,p)^{47}Sc	3.73	1.042	3.9
^{58}Ni(n,p)^{58}Co	4.12	1.088	3.5
^{46}Ti(n,p)^{46}Sc	5.98	1.273	4.0
^{56}Fe(n,p)^{56}Mn	7.46	1.367	3.2
^{48}Ti(n,p)^{48}Sc	8.22	1.460	4.2
^{197}Au(n,2n)^{196}Au	10.47	1.686	4.7
^{127}I(n,2n)^{126}I	11.51	1.718	5.5
^{89}Y(n,2n)^{88}Y	13.84	2.076	4.6
^{19}F(n,2n)^{18}F	13.96	1.973	3.8
^{58}Ni(n,2n)^{57}Ni	14.91	2.070	4.5
^{23}Na(n,2n)^{22}Na	15.37	2.211	5.4

4 Conclusions

The work presented the set of SACS ratios over the broad range of mean response energies. The results show that using ENDF/B-VIII.0 ^{235}U PFNS gives good agreement with experimental data including very high mean response energies unlike JEFF-3.3 ^{235}U PFNS. ENDF/B-VIII.0 ^{235}U PFNS has harder neutron spectrum than theoretically expected. These data can be used as a challenge for various theoretical fission models.

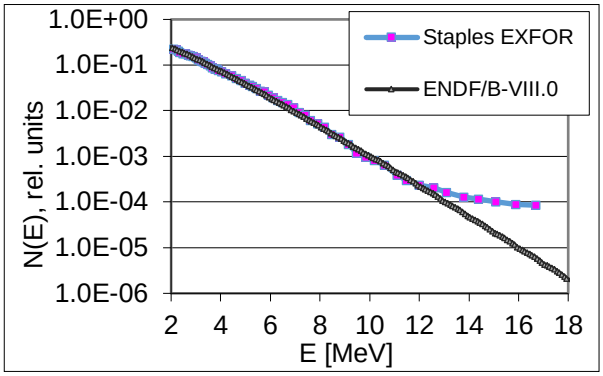

Fig. 3. Comparison of ^{235}U ENDF/B-VIII.0 PFNS with existing differential data measured by Staples.

Acknowledgement

Presented results were obtained with the use of infrastructure Reactors LVR-15 and LR-0, which is financially supported by the Ministry of Education, Youth and Sports - project LM2018120 and the SANDA project funded under H2020 EURATOM-1.1 contract 847552.

References

1. R. Capote, Y. F. Hambsch et al., Nucl. Data Sheets 131, 1-106 (2016)
2. D.A. Brown, M.B. Chadwick, R. Capote et al., Nucl. Data Sheets 148, 1-142 (2018)
3. A. Plompen, O. Cabellos, C. De Saint Jean et al., EPJ A, 56 (2020)
4. A. Trkov, P. J. Griffin, S. P. Simakov et al., Nuclear Data Sheets 163, 1-108, (2020)
5. M. Kostal, M. Schulc, E. Losa et al., Annals of Nuclear Energy 140 107119, (2019)
6. M. Kostal, V. Rypar, J. Milcak et al., Annals of Nuclear Energy 87, 601-611 (2016)
7. M. Kostal, M. Svadlenkova, P. Baron et al., Annals of Nuclear Energy 90, 450-458, (2016)
8. M. Kostal, T. Czakoj, E. Losa et al, App. Rad. Isot., 120, 45-50 (2017)
9. M. Kostal, M.Schulc, V. Rypar et al, App Rad Isot. 128, 92-100, (2017)
10. M. Kostal, M. Svadlenkova, P. Baron et al., App. Rad. Isot. 111, 1-7 (2016)
11. M. Kostal et al., LR0-RESR-004, IRPhE (2018); EXFOR 31771.006
12. M. Kostal, E. Losa, M.Schulc et al., Annals of Nuclear Energy 158 108268, (2021)
13. M. Koleska, M. Sunka and J. Ernest, Nuclear Energy and Radiation Science 2, 0145021-4 (2017)
14. M. Schulc, M. Kostal, J. Simon et al., Appl. Rad. Isot. 166, 109313 (2020)
15. M. Schulc, M. Kostal, E. Novak et al., App. Rad. Isot. 151, 187-195 (2019)
16. M. Schulc, M. Kostal, S. Simakov et al., App.Rad. Isot. 132, 29-37 (2018)
17. M. Schulc, M. Kostal, R. Capote et al., App. Rad. Isot. 143, 132-140 (2019)
18. M. Schulc, M. Kostal, J. Simon et al., App. Rad. Isot. 155, 108937 (2020)
19. M. Schulc, M. Kostal, J. Simon et al., Appl. Rad. Isot 166, 109355 (2020)
20. T. Goorley, M. James, T. Booth, F.B. Brown et al., Overview. Nucl. Technol 180, 298–315 (2012)
21. P. Staples, J.J. Egan, G.H.R. Kegel et al., Nucl. Phys. A 591 (1995).